Anti-dive Suspension Force Based Sprung Roll-Heave Non-interference Simultaneous Control of In-wheel-motored Vehicles

Qi Chen*a) Non-member, Nagai Sakahisa* Member
Binhminh Nguyen* Member, Hiroshi Fujimoto* Senior Member

Focusing on the riding comfort and safety of in-wheel-motor electric vehicles in the forward direction, integrated control of roll and heave motion is necessary. This study proposed a roll-heave simultaneous controller with actuators of only anti-dive suspension reaction forces, with decoherence of the motion control in different directions. Simulation and experiments are carried out to prove the effectiveness of the proposed method.

Keywords: Electrical Vehicle, In-wheel motor, Anti-dive Force, Roll control, Heave control

1. Introduction

1.1 Background Nowadays, with the consideration of global warming, exhaustion of fossil fuels, and pollution, electric vehicles (EVs) have attracted much more attention. In addition, EVs have some remarkable merits compared to traditional internal combustion engine vehicles, such as quick torque response and accurate measurement of motor torque [1]. Furthermore, it is possible to independently control the torque of each wheel to achieve better controllability [2], thanks to the in-wheel-motor (IWM) actuators. This feature also allows IWM-EV to achieve less mechanical resonance introduced by gears, shafts, and differentials. Based on the aforementioned features, various advanced motion control methods have been developed for IWM-EVs, such as direct yaw moment control [3], cornering force maximization [4], energy efficiency autonomous driving [5], and optimal energy management [6].

1.2 Study motivation Considering the tip-in of road disturbance on one side of the vehicle, heave and roll motion occur with the one-side vertical displacement of the wheel, which influences the riding comfort. Furthermore, with a large roll angel, the risk of rollover can not be ignored. Thus, a simultaneous control of roll and heave motion is necessary.

In previous studies [7][8], heave motion control and roll motion control are proposed individually with the use of anti-dive suspension force but the simultaneous control of both motions has not been considered yet. Multi-degree motion control including roll and heave is proposed in some research [9][10] but additional actuators like active suspensions are needed. Besides, coherence between the control of the two motions has not been discussed yet.

Focusing on the sprung motion of roll and heave below 10 Hz, the contributions of this paper can be summarized as follows:

- An integrated half-car model is developed to simultaneously analyze heave and roll motion with respect to road disturbance in Section 2.
- An integrated control system of both heave and roll motion. Especially, a new roll controller is introduced for the first time based on the idea of a skyhook controller in Section 3.
- The proposed method has been evaluated by both frequency analysis and experiment in Sections 4 and 5.

a) Correspondence to: chen-qi4396@g.ecc.u-tokyo.ac.jp
* eMobility and Control Lab, The University of Tokyo
Kashiwanoha 5 − 1 − 5, Kashiwa, Chiba, 277-0882

Table 1. Specification of the vehicle under study.

Parameters	symbol	unit	value
half sprung mass	m_2	kg	400
one-wheel unsprung mass	m_1	kg	45
suspension stiffness	k_s	N/m	20000
suspension damping	c_s	N/(m/s)	1000
tire stiffness	k_t	N/m	150000
tire damping	c_t	N/(m/s)	500
anti-dive angle of rear wheel	θ	rad	0.2
moment of roll inertia	I_x	Nm	110
tire inertia	J_w	kgm^2	1.24
tread base of rear wheel	d_r	mm	1300
height from road to CoG	h_g	mm	510

2. Modeling

The specification of the experiment vehicle suspension system is given in Table.1, where the value is given by the nominal model of our experimental plant.

2.1 Motion dynamic of forward direction Focusing on the roll and heave motion of EVs equipped with in-wheel motors, with respect to the aforementioned problem setting, the plant model can be simplified into a two-wheel model shown in Section 2.4. The horizontal driving force $F_{d,k}$ of the vehicle can be given by the function of slip ratio λ as follows:

$$F_{d,k} = f(\lambda_k) \tag{1}$$

$$\lambda_k = \frac{rw_k - v}{rw_k} \tag{2}$$

where $k = l, r$ refers to left and right wheel, λ_k is the slip ratio, r is the radius of tire, w_k is the rotation angle velocity of wheel and v is the velocity of vehicle in forward direction. The function f is given as Magic Formula [13] in certain range

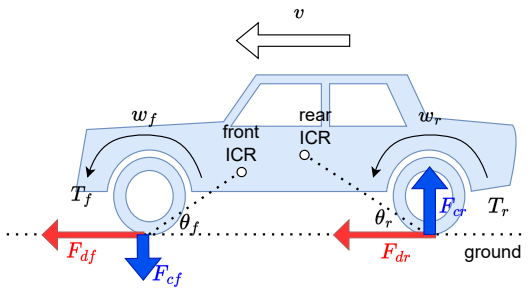

Fig. 1. Instant rotation with driving force.

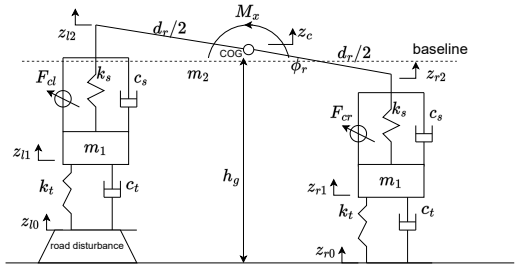

Fig. 2. Half car model of roll motion.

of λ_k.

Assuming a high-friction road condition where $\lambda_k \approx 0$, $F_{d,k}$ can be approximately expressed as the following equation:

$$F_{d,k} = \frac{T_k - J_w\dot{\omega}_k}{r} \approx \frac{T_k}{r} \tag{3}$$

where T_k refers to the torque output and J_w is the rotation moment of inertia of the wheel.

2.2 Motion dynamic of anti-dive Fig. 1 shows the anti-dive motion of the vehicle under the driving force F_d. With the characteristic of anti-dive [11] shown in Fig. 1, a instant rotation moment will be generated with the horizontal driving force F_d through the suspension arms around a rotation center called ICR (instant center of rotation). Thus the vertical anti-dive force F_c and the F_d can be expressed as follows, where the ϕ_r angle represents the anti-dive angle of the rear wheel shown in Fig. 1:

$$F_{ck} = F_{dk}\tan\theta = \frac{T_k}{r}\tan\theta \tag{4}$$

The vertical motion of the vehicle can thus be controlled by torque control without additional actuators.

2.3 Half car model Considering a one-side road disturbance tip-in (for example, the tip-in of a bump beneath the left wheel) of forward direction driving, a half-car model with the left and right diving wheel as well as the sprung mass is given as Fig. 2. As shown in Fig. 2, the motion dynamic can be divided into two parts: the unsprung vibration of the wheels m_1, and the heave and roll motion of sprung mass m_2. The dynamic equations of unsprung mass m_1 can be given as follows with the anti-dive force input F_{ck}:

$$\begin{aligned} &m_1\ddot{z}_{k1} + (c_s + c_t)\dot{z}_{k1} + (k_s + k_t)z_{k1} \\ &\quad = c_s\dot{z}_{k2} + k_s z_{k2} + c_t\dot{z}_{k0} + k_t\dot{z}_{k0} - F_{ck} \end{aligned} \tag{5}$$

where z_{k2} is the vertical displacement of the left and right end of the sprung mass and can be given as follows with the counter-clockwise roll angle to be the positive direction, where $d_0 = d_r/2$:

$$z_{2k} = z_c \pm d_0\tan\phi_r \tag{6}$$

The total vertical force on the left and right side of the sprung mass can be given as:

$$F_{zk} = F_{ck} + c_s(\dot{z}_{k1} - \dot{z}_{k2}) + k_s(z_{k1} - z_{k2}) \tag{7}$$

With (7), the heave and roll motion of sprung mass on the CoG (center of gravity) can be given as (8) and (9):

$$m_0\ddot{z}_c = F_{zl} + F_{zr} \tag{8}$$

$$I\ddot{\phi}_r = d_0(F_{zr} - F_{zl}) \tag{9}$$

With (8) and (9), the model can be given as a equation of state space $\dot{x} = Ax + Bu$, where $x = [\dot{z}_{l1}, z_{l1}, \dot{z}_{r1}, z_{r1}, \dot{z}_c, z_c, \dot{\phi}_r, \phi_r]^T$ and $u = [F_{cl}, F_{cr}, z_{l0}, z_{r0}, \dot{z}_{l0}, \dot{z}_{r0}]^T$.

3. Controller design

In this section, the convention triple skyhook (tSH) heave motion control [7] is first introduced. Then, a novel skyhook-based roll controller expanded from tSH control is proposed. And the interference between the two motions of heave and roll control is discussed.

3.1 Outline of proposal method The block of the heave-roll simultaneous controller in this study is given in Fig. 3. Here, a band-pass filter with cutoff frequency on $1 - 10$ Hz is first given to decrease the sensor noise and offset [12]. The plant model is given by (8) and (9). The vibration controller is given by the study of triple skyhook control [7], which will be discussed below. As is shown in Fig. 4, assuming that no roll moment is generated with the assumption of the following equation:

$$d_0F_{clv} = d_0F_{crv} \tag{10}$$

Thus $F_{clv} = F_{crv} = F_{cv}$ can be used as the heave control input. Here, a simplified 1-DOF heave motion model without the consideration of unsprung characteristics is given in Fig. 5, and the motion dynamic of the heave motion can be given as follows:

$$m_2\ddot{z}_c = 2F_{cv} + 2c_s(\dot{z}_1 - \dot{z}_2) + 2k_s(z_1 - z_2) \tag{11}$$

With (11), the transfer function from the unsprung vertical displacement z_1 to the sprung vertical displacement z_c can be given as follows:

$$z_c = \frac{2c_s s + k_s}{m_2 s^2 + 2c_s s + 2k_s}z_1 + \frac{2}{m_2 s^2 + 2c_s s + 2k_s}F_{cv} \tag{12}$$

From (12), the controller for heave motion can be designed as:

$$V_{pl,r} = \frac{F_{cvl,r}}{z_c} = -\frac{\beta_v}{2}(m_2 s^2 + 2c_s s + 2k_s) \tag{13}$$

Where l, r represent the left and right, respectively. And the heave of z_c can be suppressed ideally as follows:

$$z_c = \frac{1}{1 + \beta_v}\frac{2c_s s + k_s}{m_2 s^2 + 2c_s s + 2k_s}z_1 \tag{14}$$

The controller's (13) is also known as "triple skyhook (tSH) control" in the previous study, which is proposed for a quarter-car model to suppress the heave motion below 10 Hz with anti-dive force. However, the consideration of other sprung motions has not been taken yet.

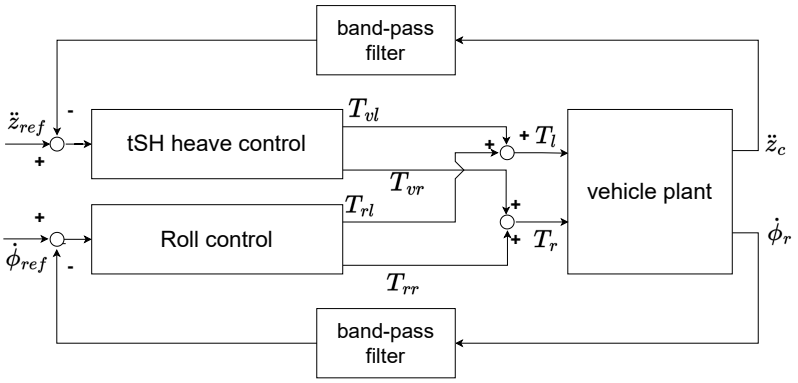

Fig. 3. Block diagram of the heave-roll simultaneous controller.

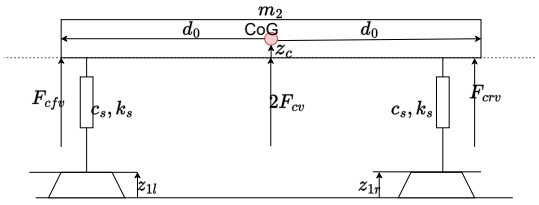

Fig. 4. Motion decomposition of heave.

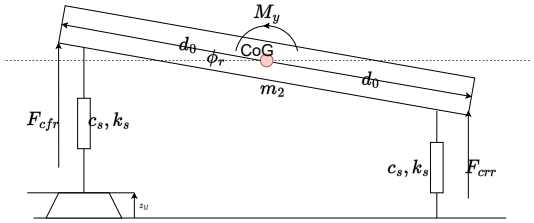

Fig. 5. Motion decomposition of the roll motion.

3.2 Proposal skyhook-based roll motion control

Considering a non-heave motion model as Fig. 5 with a tip-in of road disturbance on the left side, where

$$F_{clr} + F_{crr} = 0 \tag{15}$$

Assuming that $F_{crr} = -F_{clr} = F_{croll}$, the motion dynamic for Fig. 2 can be described as:

$$I_x\ddot{\phi}_r = 2d_0F_{croll} - d_0c_s\dot{z}_1 - d_0k_sz_1 + 2d_0^2c_s\dot{\phi}_r + 2d_0^2k_s\phi_r \tag{16}$$

Thus, the transfer function from z_1 to ϕ_r can be given as follows:

$$\phi_r = -\frac{d_0(c_ss + k_s)}{I_xs^2 + 2d_0^2c_ss + 2d_0^2k_s}z_1 + \frac{2d_0}{I_xs^2 + 2d_0^2c_ss + 2d_0^2k_s}F_{croll} \cdots\cdots\cdots\cdots \tag{17}$$

From (17), the controller of roll motion can be given as (18), with the roll motion suppressed ideally as (19):

$$R_{pl,r} = \frac{F_{crolll,r}}{\phi_r} = \pm\frac{\beta_r}{2d_0}(I_xs^2 + 2d_0^2c_ss + 2d_0^2k_s) \tag{18}$$

$$\phi_r = -\frac{1}{1+\beta_r}\frac{d_0(c_ss + k_s)}{I_xs^2 + 2d_0^2c_ss + 2d_0^2k_s}z_1 \tag{19}$$

Here, the right side is given as the positive side. Similarly, the controller (18) works the same when there is a z_1 displacement input on the right side.

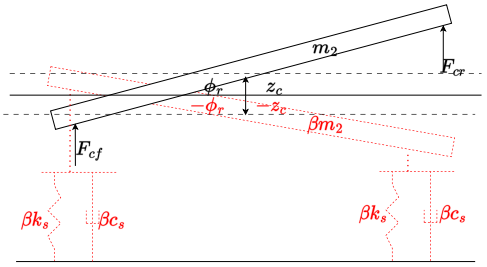

Fig. 6. Physical characteristics of the proposal controller.

Thus, the proposal 2-DOF control, the novel roll controller (18) combined with the tSH control (13), can be given as (20) and (21) with the assumption of $\beta_r = \beta_v = \beta$:

$$F_{cl} = F_{cv} + F_{crolll} \tag{20}$$

$$F_{cr} = F_{cv} + F_{crollr} \tag{21}$$

With (4), the torque control of the left and right rear wheels can be given as follows:

$$T_{cl,r} = \frac{r\beta}{\tan\theta}(-\frac{1}{2}(m_2s^2 + 2c_ss + 2k_s)z_c \pm \frac{1}{2d_0}(I_xs^2 + 2d_0^2c_ss + 2d_0^2k_s)\phi_r) \cdots\cdots\cdots\cdots \tag{22}$$

As is shown in Fig. 6, for the real heave and roll motion of the black sprung mass, the proposal method provides a virtual actuator with the same structures of left and right suspensions as well as the sprung mass shown in red and generates a reverse movement of the real plant. Thus the heave and roll motion can be suppressed at the same time.

3.3 Interference between roll and heave control

For an two-input-two-output control system of suspension reaction force to heave and roll motion, the transfer function of control input can be given as follows:

$$\begin{pmatrix} F_{cl} \\ F_{cr} \end{pmatrix} = \begin{pmatrix} V_l & R_l \\ V_r & R_r \end{pmatrix}\begin{pmatrix} z_c \\ \phi_r \end{pmatrix} = R\begin{pmatrix} z_c \\ \phi_r \end{pmatrix} \tag{23}$$

Where V_l, V_r refer to the transfer function from the feedback vertical vibration z_c to the vertical forces, and R_f, R_r refer to the transfer function from the feedback roll motion ϕ_r to the vertical forces of each wheel. In our proposed method, the V_l, V_r is given as (13) and R_f, R_r is given as (18).

The influence from $(F_{cl}, F_{cr})^T$ to plant motion variation $(\Delta z_c, \Delta\phi_r)^T$ can not be calculated directly if the R matrix here

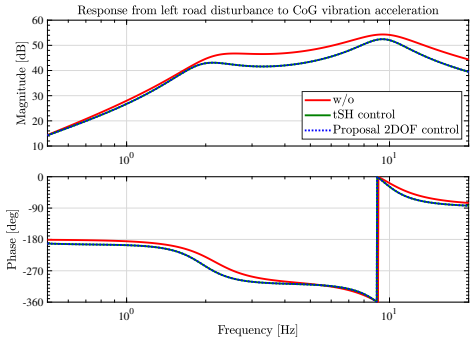

Fig. 7. Frequency response of heave motion.

Table 2. Parameters of controllers.

controller parameters	symbol	value
Poles of conventional PI control	$p_{1,2}$	-15 rad/s
cutoff frequency of HPF	f_h	1 Hz
cutoff frequency of LPF	f_l	10Hz
heave acceleration reference	$\ddot{z}_{c,ref}$	0
roll angular speed reference	$\dot{\phi}_{r,ref}$	0
skyhook controller gain	β	0.4

is irreversible, which also means the decoherence of the motion control in different directions is impossible.

In our proposal method, the anti-dive force of the left and right wheels can be also transferred into the vertical force input F_{cv} and roll moment input M_{cx} with the following linear transformation given by (24) and (25):

$$\begin{pmatrix} F_{cv} \\ M_{cx} \end{pmatrix} = \begin{pmatrix} 1/2 & 1/2 \\ -l_f & l_r \end{pmatrix} \begin{pmatrix} F_{cl} \\ F_{cr} \end{pmatrix} = S \begin{pmatrix} F_{cl} \\ F_{cr} \end{pmatrix} \quad (24)$$

Thus, (23) can be rewritten as follows:

$$\begin{pmatrix} F_{cv} \\ M_{cx} \end{pmatrix} = \begin{pmatrix} V_0 & 0 \\ 0 & R_0 \end{pmatrix} \begin{pmatrix} z_c \\ \phi_r \end{pmatrix} = T \begin{pmatrix} z_c \\ \phi_r \end{pmatrix} \quad (25)$$

where $V_0 = -\beta_v(m_2 s^2 + 2c_s s + 2k_s), R_0 = -\beta_r(I_x s^2 + d_0 c_s s + d_0 k_s)$ are the transfer functions given by (13) and (18). Thus, the plant motion variation $(\Delta z_c, \Delta\phi_r)^T$ influenced by the control input can be given as:

$$\begin{pmatrix} \Delta z_c \\ \Delta\phi_r \end{pmatrix} = T^{-1} S \begin{pmatrix} F_{cl} \\ F_{cr} \end{pmatrix} \quad (26)$$

With (26), the motion variation of the vehicle plant can always be solved individually in different directions.

Frequency response from road disturbance beneath left wheel z_{l0} to the heave acceleration $\ddot{z}_c$ with only tSH heave control and tSH+proposal roll control is shown in Fig. 7. It is clear that the add-in of the proposal roll controller has no weakening of the vibration control, which proves the decoherence of the motion control on heave and roll directions.

4. Simulation Evaluation

4.1 Simulation setup In this section, the algorithm is evaluated with the parameters in Table.2. As a comparison, a roll-moment-observer-based (RMO-based) roll moment control [8] with anti-dive force is taken as the conventional roll control method, as the block diagram shown in Fig. 8. The parameters of the controllers are given in the Table.2

Here, a PI controller is given as the feedback roll moment control. The band-pass filter is the same as the proposal

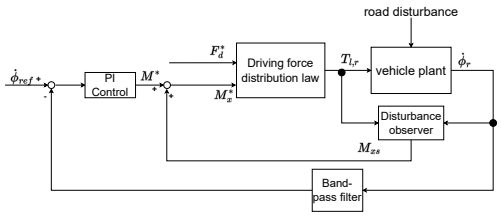

Fig. 8. Block diagram of the conventional method.

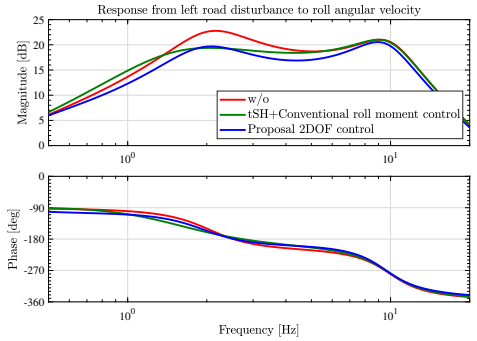

Fig. 9. Frequency response of roll motion.

method. The F_d^* refers to the driving force input by other controllers, and here, it mainly consists of velocity control output and tSH heave control output. The driving force distribution law given in the previous research is a least-squares method by equalization of the tire load with the least-squares method. Besides, a disturbance observer is used in this method to suppress the influence of disturbance and model parameter error, with the compensating roll moment M_{xs} calculated by comparing the reference moment M_{xr} given by torque input and the nominal moment M_{xn} conducted from the roll angular velocity.

The controller gain β is limited by the maximum torque output of our test vehicle [12] and given as the table. Both of the conventional and proposed roll controllers are combined with the tSH heave control in the simulation and the experiments to evaluate the performance of roll-heave simultaneous control.

4.2 Simulation of roll angular velocity suppression The frequency response from z_{l0} to the roll angular velocity $\dot{\phi}_r$ is given in Fig. 9. Here, the bode response of the conventional method is given without the non-linear driving force distribution block, remaining only a linear roll moment control system.

As shown in the figure, the conventional RMO-based method can only suppress the roll motion around 1.5 – 4 Hz, which is limited by the pole of the PI controller (−15 rad). By adjusting the pole of the PI roll moment controller, the conventional method can be effective around different frequency ranges, but the rest parts below 10 Hz will be the same as the case without control, or even get worsen, as the part below 1.5 Hz shown in Fig. 9. In comparison, our proposal method has suppressed the roll motion and always shows better performance than the conventional method in all of the frequency range below 10 Hz.

However, the time response given in Fig. 10 with the conventional and proposal roll control combined with the same tSH heave control shows that considering the influence of

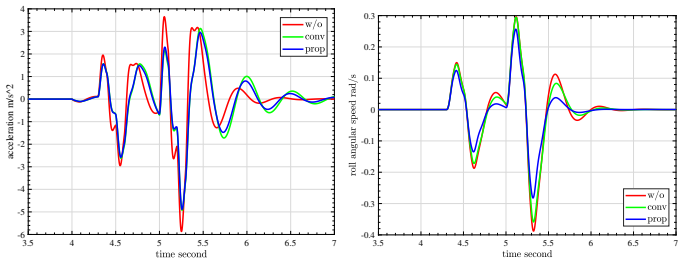

(a) Heave acceleration response. (b) Roll angular velocity response

Fig. 10. Time response of heave and roll motions.

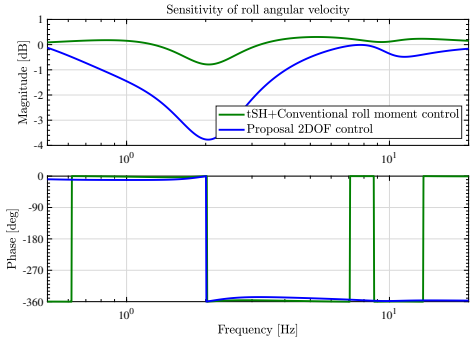

Fig. 11. Sensitivity of roll angular velocity.

heave control and the driving force distribution algorithm, the conventional method shows little effectiveness on roll control and get a little worse in heave control due to the non-linear interference between the heave and roll motion control. On the opposite, our proposed method performs well in both heave and roll control.

4.3 Sensitivity of roll angular velocity Considering the sensitivity function of roll angular velocity as follows.

$$S_{roll} = \frac{1}{1 + C(s)P(s)} \tag{27}$$

Where the $P(s)$ is the half-car plant model transfer function from road displacement (here, the displacement under left side for example) given by the status space equation given in Section 2, and $C(s)$ refers to the conventional and proposal roll control method.

As shown in Fig. 11, the proposal method shows lower sensitivity than the conventional method all over the frequency band below 10 Hz, especially around the resonance frequency of the sprung mass, where both of the controllers show the same performance in the roll suppression as Fig. 9. Thus, it can be conducted that though the controllers perform nearly the same on the 1.5 – 4 Hz frequency range in theory, the proposal method will show more robustness and effectiveness than the conventional method in practice.

5. Experiment

5.1 Experimental EV The in-wheel-motor-equipped electric vehicle FPEV-2 Kanon (in the left of Fig. 12) is developed by our group for performance verification. The left and rear wheels can be controlled individually with a maximum torque output of 340 Nm for each wheel in both front and rear directions. Three-axis IMU and gyro sensors setting on the center of gravity are used to provide x, y, and z-axis acceleration and the pitching-roll-yaw angular velocity.

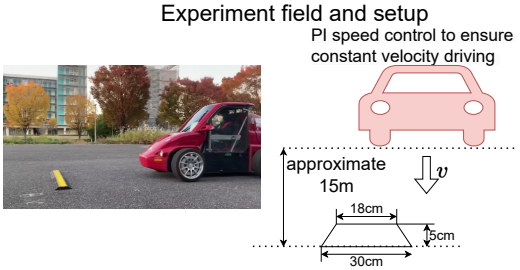

Fig. 12. Experimental setup.

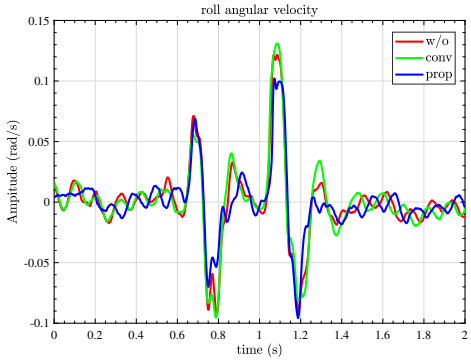

(a) Result of sprung roll angular speed.

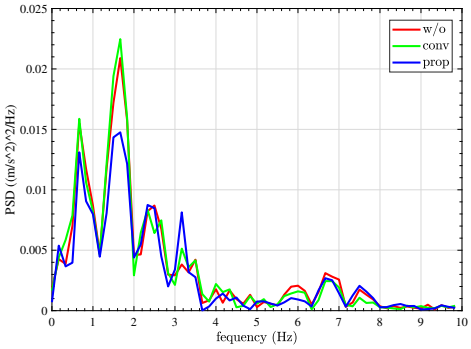

(b) PSD of sprung roll angular speed.

Fig. 13. Result of roll angular velocity.

5.2 Experimental setup To evaluate our method, a driving-over-bump experiment was conducted as the condition shown in Fig. 12 with the experimental vehicle FPEV2-Kanon run over a bump on one side at a speed of 2.5 m/s. The test was repeated five times for the conventional disturbance observer-based method combined with the tSH control, and our proposed heave-roll simultaneous controller to compare to the non-control situation. The control period and sensor sampling period were chosen as 1 ms. Root mean square error (RMSE) for each test group was calculated for evaluating and comparing the methods, where zero-vibration input is used as the reference. The T-test of each experiments group are taken to evaluate the credibility of how the raw data deviating from the average data, and the P-value of the T-test in each group are calculated.

5.3 Experiment result

5.3.1 Result of sprung roll angular velocity Fig. 13 and Table.3 shows the roll angular velocity results of the experiment. The PSD of the data shows that the conventional roll controller shows the tendency of getting worse above

Table 3. Data of experiments.

		Average P-to-P	Error range	RMSE	P-value
Roll	w/o	0.214 rad/s	-0.021 to +0.015	0.033	0.905
	Conv	0.223 rad/s	-0.024 to +0.017	0.034	0.862
	Prop	0.198 rad/s	-0.007 to +0.012	0.028	0.941
Heave	w/o	4.03 m/s^2	-0.19 to +0.21	0.485	0.849
	Conv	3.91 m/s^2	-0.18 to +0.26	0.511	0.907
	Prop	3.7 m/s^2	-0.17 to +0.21	0.427	0.929

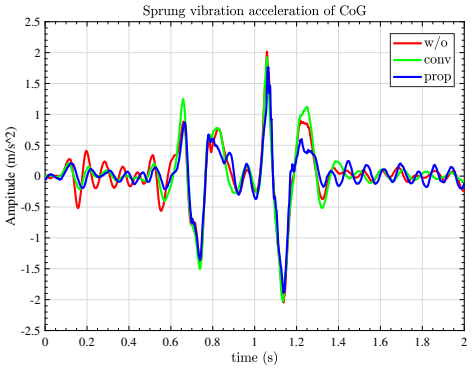

(a) Measurement of sprung heave acceleration.

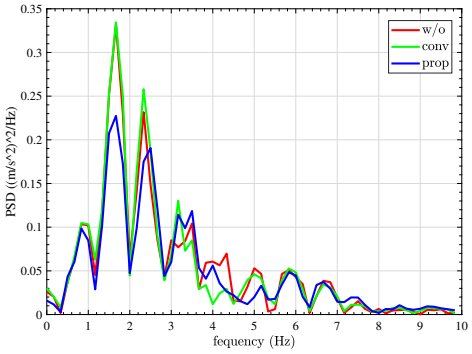

(b) PSD of sprung heave acceleration.

Fig. 14. Result of heave acceleration.

4 Hz and achieves only a little effectiveness in low frequency, which makes the peak-to-peak roll angular velocity with the conventional method enhanced by 4.8 % in total. On the other hand, our proposal method shows a good performance around 1.5 Hz, the same as the simulation, and achieves a total roll angular speed suppression by 7.8 %.

5.3.2 Result of sprung heave acceleration Fig. 14 and Table.3 shows the results of heave motion. With the potential interference between roll and heave motion control, the conventional method performs well in $3-6$ Hz but badly around 2 Hz, with a total peak-to-peak vibration acceleration decrease of only 2.9 % compared to the non-control group. In comparison, our proposal method shows good performance in both $1-3$ Hz and $4-6$ Hz according to the PSD result, which makes the proposal method achieves an 8.1 % vibration suppression result and proves there is less influence between the proposal roll control and the tSH heave control.

6. Conclusion

To avoid the bandwidth limit and the interference of heave and roll motion control of EV sprung mass, this study proposed a novel roll angle controller based on the tSH vibration control and combined the two motions of the roll-heave controller without interference. Simulation and experiments are given to prove the effectiveness of our method.

With the non-interference control algorithm, additional robust controllers like disturbance observers may be added into our method in the future work. Also, only the sprung vertical motions are taken consideration in this study, remaining the combination of the considerations on other driving elements such as steering robustness, tire load minimization and so on.

References

(1) X. Sun, Z. Li, X. Wang, and C. Li, “Technology development of electric vehicles: A review,” Energies, vol.13, no.1, p.90, (2019).

(2) Oomen, Tom. ”Advanced motion control for precision mechatronics: Control, identification, and learning of complex systems.” IEEJ Journal of Industry Applications 7.2 (2018): 127-140.

(3) Takumi Ueno, Binh-Minh Nguyen, Hiroshi Fujimoto: ”Direct Yaw Moment Control for Electric Vehicles with Variable-Rate-Slip-Ratio-Limiter Based Driving Force Control”, IEEE International Conference on Mechatronics 2023, Loughborough, UK (2023).

(4) H. Fuse, H. Fujimoto: “Cornering Force Maximization with Variable Slip Ratio Control Based on Brush Tire Model ’’ , 5th International Electric Vehicle Technology Conference 2021, Online (2021).

(5) Mitsuhiro Hattori, Hiroshi Fujimoto, Yoich Hori, Yusuke Takeda, Koji Sato: “Simple Tuning and Low Computation Cost Controller for Improving Energy Efficiency of Autonomous Driving Electric Vehicle ’’ ,IEEJ Journal of Industry Applications, Vol. 9, No. 4, pp.358-365, (2020)

(6) B.-M. Nguyen, J. P. F. Trovão, and M. C. Ta. ”Double-Layer Energy Management for Multi-Motor Electric Vehicles.” IEEE Transactions on Vehicular Technology. vol. 72, no. 7, pp. 8623-8635 (2023).

(7) E. Katsuyama, “Improvement of ride comfort by triple skyhook control,” in 9th International Munich Chassis Symposium 2018. Springer, 2019, pp. 215–234. (2019)

(8) Ochi Naoya, Hiroshi Fujimoto, and Yoichi Hori. ”Proposal of roll angle control method using positive and negative anti-dive force for electric vehicle with four in-wheel motors.” 2013 IEEE International Conference on Mechatronics (ICM). IEEE, 2013.

(9) Soni, Tukesh, and Ranjana Sodhi. ”Impact of harmonic road disturbances on active magnetic bearing supported flywheel energy storage system in electric vehicles.” 2019 IEEE Transportation Electrification Conference (ITEC-India). IEEE, 2019.

(10) Ivanov Valentin, et al. ”Ride blending control for electric vehicles.” Proceedings of the 31st International Electric Vehicles Symposium & Exhibition (EVS 31), Kobe, Japan. Vol. 30. 2018.

(11) Azman, M., Rahnejat, H., King, P. D., & Gordon, T. J. (2004). Influence of anti-dive and anti-squat geometry in combined vehicle bounce and pitch dynamics. Proceedings of the Institution of Mechanical Engineers, Part K: Journal of Multi-body Dynamics, 218(4), 231-242.

(12) Qi Chen, Binhminh Nguyen, Sakahisa Nagai and Hiroshi Fujimoto, “Vertical Vibration Suppression Control Using Disturbance Observer for In-wheel Motor EV Considering Unsprung Motion”, IEE Japan Joint Technical Meeting on ”Motor Drive” ,”Rotating Machinery” and ”Vehicle Technology”, Tokyo, (2023).

(13) Pacejka, Hans B., and Egbert Bakker. ”The magic formula tyre model.” Vehicle system dynamics 21.S1 (1992): 1-18.